Report no.
UC SESM 76-5

STRUCTURAL ENGINEERING AND STRUCTURAL MECHANICS

A FINITE ELEMENT MODEL OF FLUID FLOW IN SYSTEMS OF DEFORMABLE FRACTURED ROCK

by

HANS M. HILBER
ROBERT L. TAYLOR

NOVEMBER 1976

DEPARTMENT OF CIVIL ENGINEERING
UNIVERSITY OF CALIFORNIA
BERKELEY, CALIFORNIA

BIBLIOGRAPHIC DATA SHEET	1. Report No. UC SESM 76-5	2.	3. Recipient's Accession No.
4. Title and Subtitle A FINITE ELEMENT MODEL OF FLUID FLOW IN SYSTEMS OF DEFORMABLE FRACTURED ROCK			5. Report Date November 1976 6.
7. Author(s) Hans M. Hilber and Robert L. Taylor			8. Performing Organization Rept. No.
9. Performing Organization Name and Address Department of Civil Engineering Division of Structural Engineering and Structural Mechanics University of California, Berkeley, CA 94720			10. Project/Task/Work Unit No. 11. Contract/Grant No. GK-42776
12. Sponsoring Organization Name and Address National Science Foundation			13. Type of Report & Period Covered 14.

15. Supplementary Notes

None

16. Abstracts We introduce a two-dimensional finite element model of fluid flow in fractured rock masses wherein the discontinuities are deformable and constitute the primary flow paths. The interaction between the fluid and the fracture motions as well as inertia effects are taken into account. The model permits us to simulate fractured rock systems which are at an incipient state of instability; it is possible to predict the behavior of such systems when their state of stress is changed by injection or removal of fluid.

A computer program based on this theory has been developed. It determines the hydrodynamic state of the fluid, the displacement, strain and stress response histories of the rock masses, the change of the kinetic & the potential energy of the rock, & the amount of energy dissipated during slip. A number of simplified problems are solved. The results confirm that the present model can be used to study the controlled release of tectonic stresses along predetermined faults through fluid injection.

17. Key Words and Document Analysis. 17a. Descriptors

17b. Identifiers/Open-Ended Terms

17c. COSATI Field/Group

18. Availability Statement	19. Security Class (This Report)	21. No. of Pages
Available to the general public	UNCLASSIFIED	
	20. Security Class (This Page) UNCLASSIFIED	

Department of Civil Engineering
Division of Structural Engineering
and Structural Mechanics

Report No. 76-5

A FINITE ELEMENT MODEL OF FLUID FLOW IN SYSTEMS OF DEFORMABLE FRACTURED ROCK

by

Hans M. Hilber and Robert L. Taylor

Report to

National Science Foundation

University of California
Berkeley, California

November 1976

1a

ABSTRACT

We introduce a two-dimensional finite element model of fluid flow in fractured rock masses wherein the discontinuities are deformable and constitute the primary flow paths. The interaction between the fluid and the fracture motions as well as inertia effects are taken into account. The model permits us to simulate fractured rock systems which are at an incipient state of instability; it is possible to predict the behavior of such systems when their state of stress is changed by injection or removal of fluid.

A computer program based on this theory has been developed. It determines the hydrodynamic state of the fluid, the displacement, strain and stress response histories of the rock masses, the change of the kinetic and the potential energy of the rock, and the amount of energy dissipated during slip. A number of simplified problems are solved. The results confirm that the present model can be used to study the controlled release of tectonic stresses along predetermined faults through fluid injection.

TABLE OF CONTENTS

ACKNOWLEDGEMENT

We would like to acknowledge the support for this work provided by the National Science Foundation under contract number GK-42776. We thank Ellen McKeon for typing and editing the manuscript.

1. INTRODUCTION

Considerable evidence, gathered recently at Rangely, Colorado oil field, strongly suggests that fluid injection has caused small earthquakes along a fault. This and similar observations are described by Dietrich, Raleigh and Bredehoeft [1] and Handin and Raleigh [3], among others. Consequently the concept was developed that if earthquakes can be made by man's injection of fluid into the subsurface, then perhaps the appropriate control of fluid pressures in the earth's crust can lead to a method of earthquake control along major faults [3]. In order to study the role of fluids in controlling the behavior of fractured rock masses, it is necessary to develop both mathematical models and corresponding computer programs that allow the engineer to simulate the behavior of such systems under a wide range of field conditions.

Recently several attempts at developing appropriate mathematical models have been reported [4-10]. Gale, Taylor, Witherspoon and Ayatollahi [8], modifying the two-dimensional finite element formulation described in [6,7], successfully simulated quasi-static processes in systems of deformable fractured rock wherein the discontinuities constitute the dominant flow paths. However, the dynamic nature of slip mechanisms limit the applicability of the quasi-static model to the study of pre-failure conditions. Dietrich et al. [1,2] developed a dynamic finite element model for a single fault that undergoes slip under the influence of tectonic and predetermined fluid stresses. This model is able to provide a basis for predicting the dependence of displacements and near field transient motions on stress drop, rupture dimensions and seismic energy. However, Dietrich's model was not designed to incorporate the interactive processes between the fluid pressure, the fracture deformations and the stresses in the rock.

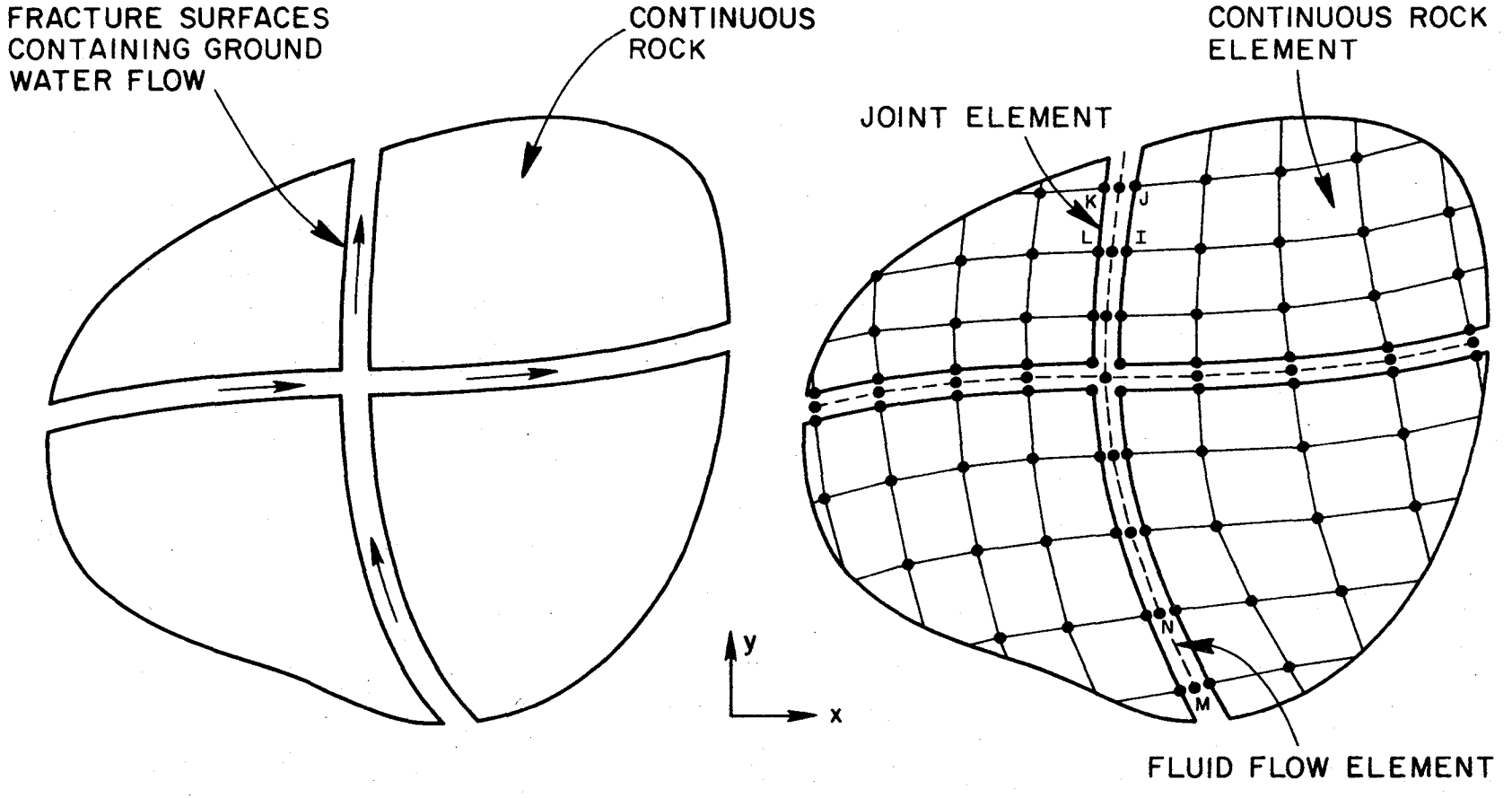

TYPICAL DETAIL OF A SYSTEM OF FRACTURED ROCK

FINITE ELEMENT MESH OF A SYSTEM OF FRACTURED ROCK

Fig. 1. Detail of an idealized two-dimensional region of a fractured rock system.

use standard step-by-step integration methods of structural dynamics to replace the differential equations by approximating algebraic equations of recursive form. Furthermore, we discuss suitable iterative techniques to solve these nonlinear equations in each time step.

Chapter 5 presents five applications of this finite element model to simplified problems in order to demonstrate some of its pertinent properties. Conclusions from this investigation are summarized in Chapter 6.

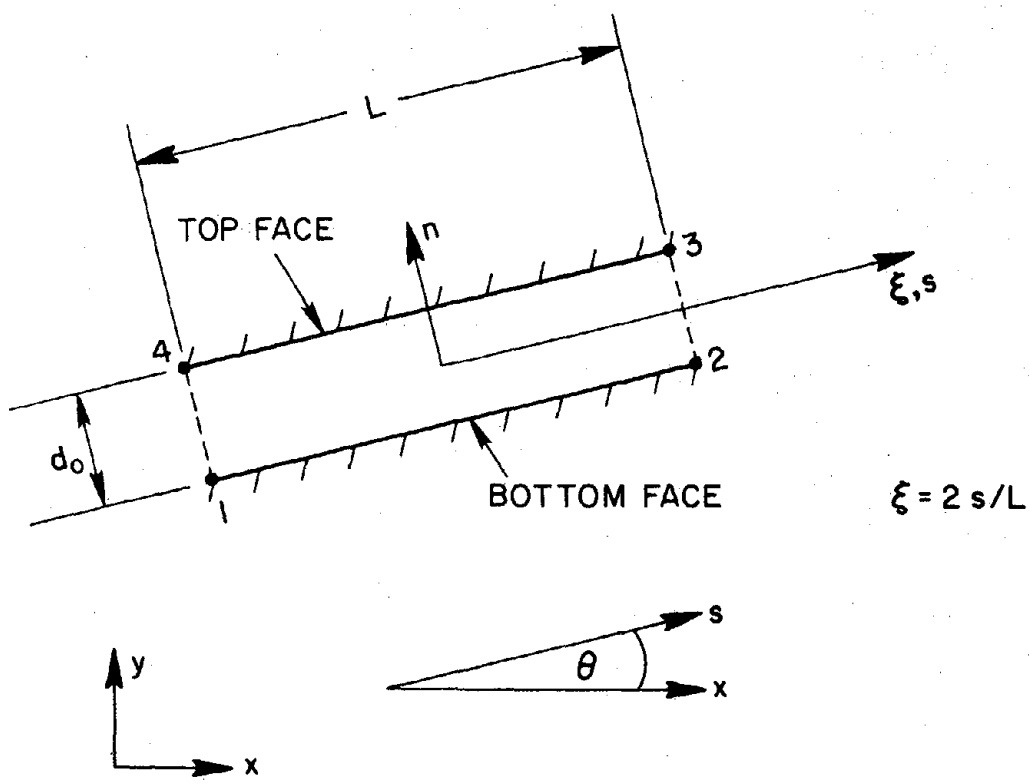

Fig. 2. Geometry and coordinate systems of the undeformed joint element.

$$\underset{\sim}{\rho}_n = \underset{\sim}{a}_n \, \underset{\sim}{C} \, \underset{\sim}{\rho} \quad , \tag{2.8c}$$

where

$$\underset{\sim}{C} = \text{diag}(\underset{\sim}{c}, \underset{\sim}{c}, \underset{\sim}{c}, \underset{\sim}{c}) \quad , \tag{2.8d}$$

and $\underset{\sim}{a}_s$ and $\underset{\sim}{a}_n$ are Boolean matrices, the elements of which are either 1 or 0; for example,

$$\underset{\sim}{a}_s = \begin{bmatrix} 1 & . & . & . & . & . & . \\ . & . & 1 & . & . & . & . \\ . & . & . & . & 1 & . & . \\ . & . & . & . & . & . & 1 \end{bmatrix} \quad . \tag{2.8e}$$

Next we define the constitutive model of the joint material. To this end we introduce the vectors

$$\underset{\sim}{\varepsilon} = (\varepsilon_s, \varepsilon_n)^T \quad , \tag{2.10a}$$

$$\underset{\sim}{f} = (f_s, f_n)^T \quad , \tag{2.10b}$$

where the elements of $\underset{\sim}{\varepsilon}$ are defined by (2.4), and f_s and f_n are shear and normal forces per unit length acting in directions s and n, respectively. Constitutive theories of discontinuities in rock defining the relation between $\underset{\sim}{f}$ and $\underset{\sim}{\varepsilon}$ were discussed by Goodman and Dubois [9]. In the present work the mechanical behavior of jointed rock is described by a nondilatant model in which shear and normal deformations are locally uncoupled. However, shear and normal modes of deformations are coupled indirectly through a Coulomb type failure criterion, as will be seen later. Goodman, Taylor and Brekke [7] proposed a constitutive model similar to the one introduced here.

In accordance with the experimental data reviewed in [9], the normal stress is related to the normal strain by an elastic, (i.e. path independent and nondissipative) law of the form

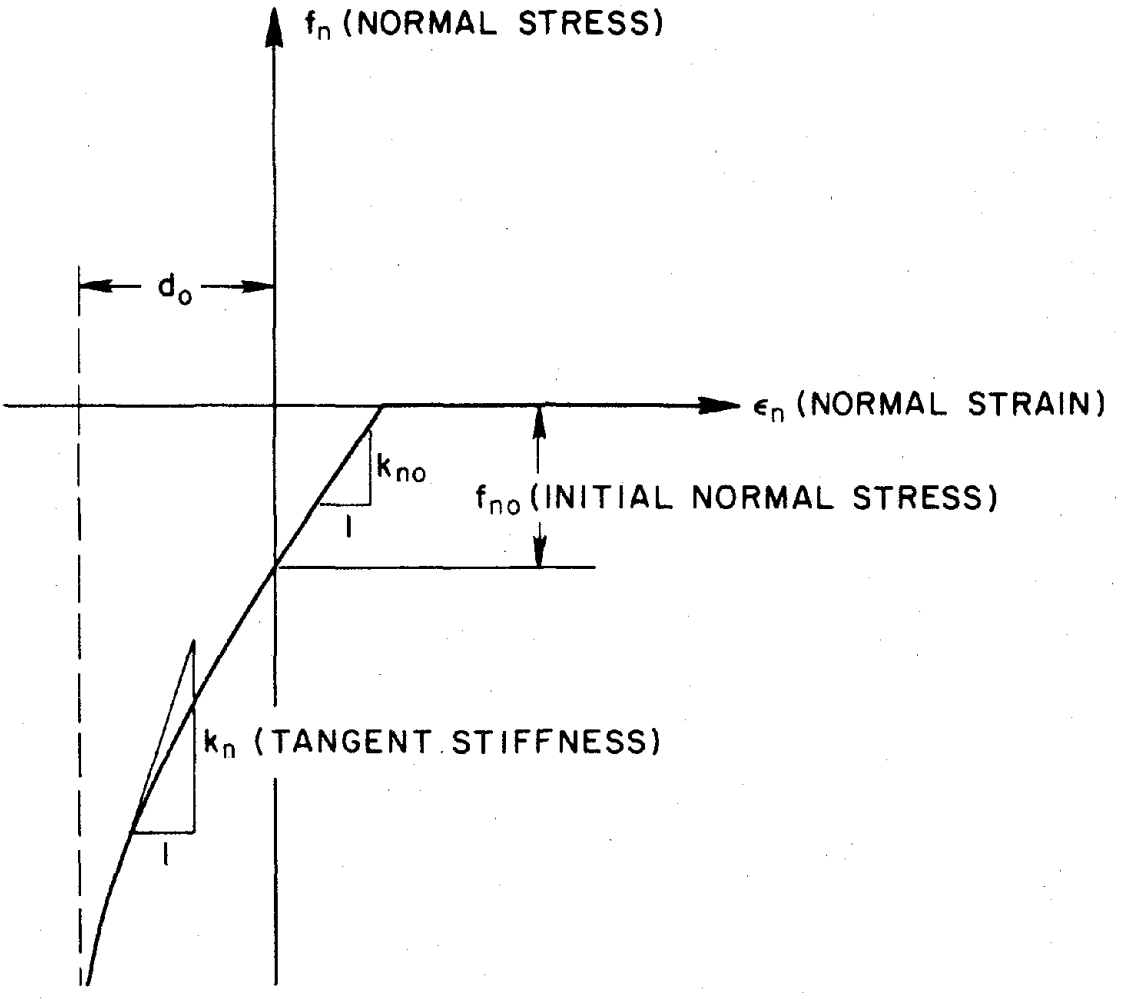

DEFINITION OF THE CONSTITUTIVE RELATION $f_n(\varepsilon_n)$:

$$-d_o < \varepsilon_n \leq 0: \qquad f_n = f_{no} + \frac{k_{no}\,\varepsilon_n}{1 + \varepsilon_n/d_o}\,, \qquad k_n = \frac{k_{no}}{(1 + \varepsilon_n/d_o)^2}$$

$$0 \leq \varepsilon_n \leq -\frac{f_{no}}{k_{no}}: \qquad f_n = f_{no} + k_{no}\,\varepsilon_n\,, \qquad k_n = k_{no}$$

$$-\frac{f_{no}}{k_{no}} < \varepsilon_n: \qquad f_n = 0\,, \qquad k_n = 0$$

Fig. 3. Constitutive relation of joint element in contacting mode of deformation.

where

$$\underset{\sim}{D} = \begin{bmatrix} -sc & sc & 0 & c^2 - s^2 \\ s^2 & c^2 & 0 & -2sc \end{bmatrix}, \tag{2.14b}$$

and $s = \sin\Theta$, $c = \cos\Theta$. Equations (2.14) are used to define the initial state of stress of a fracture surface such that it is statically compatible with the corresponding initial state of stress of the adjacent continuum.

Next we introduce the vector of nodal forces in global directions

$$\underset{\sim}{P} = (P_{x1}, P_{y1}, \ldots, P_{x4}, P_{y4})^T \quad , \tag{2.15}$$

and the vectors

$$\left.\begin{aligned} \underset{\sim s}{P} &= (P_{s1}, P_{s2}, P_{s3}, P_{s4})^T \\ \underset{\sim n}{P} &= (P_{n1}, P_{n2}, P_{n3}, P_{n4})^T \end{aligned}\right\} \quad , \tag{2.16}$$

where, for example, P_{s1} is the force at node 1 in direction s. The vector $\underset{\sim}{P}$ is related to $\underset{\sim s}{P}$ and $\underset{\sim n}{P}$ by the equilibrium equation

$$\underset{\sim}{P} = \underset{\sim}{C}^T (\underset{\sim s}{a}^T \underset{\sim s}{P} + \underset{\sim n}{a}^T \underset{\sim n}{P}), \tag{2.17}$$

and matrices $\underset{\sim}{C}$, $\underset{\sim s}{a}$ and $\underset{\sim n}{a}$ have been defined above; see expressions (2.8).

We want to establish the conditions of equilibrium between the nodal forces and the internal state of stress. By the principle of virtual displacements

$$\left.\begin{aligned} \underset{\sim s}{P} &= \frac{L}{2} \int_{-1}^{1} \underset{\sim}{\phi}^T f_s \, d\xi \\ \underset{\sim n}{P} &= \frac{L}{2} \int_{-1}^{1} \underset{\sim}{\phi}^T f_n \, d\xi \end{aligned}\right\} \quad . \tag{2.18}$$

$$\left.\begin{aligned} \underset{\sim}{k}_s &= \frac{L}{2}\int_{-1}^{1} k_s\, \underset{\sim}{\phi}^T\, \underset{\sim}{\phi}\, d\xi \\ \underset{\sim}{k}_n &= \frac{L}{2}\int_{-1}^{1} k_n\, \underset{\sim}{\phi}^T\, \underset{\sim}{\phi}\, d\xi \end{aligned}\right\} \quad . \tag{2.23}$$

The mass density of material contained between slip surfaces is usually negligible compared to the density of the surrounding rock. Accordingly, we assume the joint element to have no mass.

The sum of the strain energy and the dissipated energy is defined by

$$U + E_D = \frac{L}{2}\int_{-1}^{1}\int_{\underset{\sim}{0}}^{\underset{\sim}{\varepsilon}} \underset{\sim}{f}^T\, d\underset{\sim}{\varepsilon}\, d\xi \quad . \tag{2.24}$$

Substituting (2.10) into (2.24), and making use of (2.5) and (2.18), we obtain

$$U + E_D = \int_{\underset{\sim}{0}}^{\underset{\sim}{\rho}_s} \underset{\sim}{P}_s^T\, d\underset{\sim}{\rho}_s + \int_{\underset{\sim}{0}}^{\underset{\sim}{\rho}_n} \underset{\sim}{P}_n^T\, d\underset{\sim}{\rho}_n \quad . \tag{2.25}$$

The shear behavior is governed by the elastic-plastic constitutive model defined in Figure 4. Correspondingly, we can decompose the shear strains into elastic and plastic components:

$$\varepsilon_s = \varepsilon_s^e + \varepsilon_s^p \quad . \tag{2.26}$$

In view of (2.4), (2.19) and (2.26) the strain energy

$$U = \int_0^{\varepsilon_{s1}^e} P_{s4}\, d\varepsilon_{s1}^e + \int_0^{\varepsilon_{s2}^e} P_{s3}\, d\varepsilon_{s2}^e + \int_0^{\varepsilon_{n1}} P_{n4}\, d\varepsilon_{n1} + \int_0^{\varepsilon_{n2}} P_{n3}\, d\varepsilon_{n2} \tag{2.27a}$$

and the dissipated energy

Next we discuss methods for computing the vectors of internal forces (2.18) and the stiffness matrices (2.23). The integrals in equations (2.18) and (2.23) are most conveniently evaluated numerically. A two-point integration rule was found to be adequate in terms of accuracy and computational efficiency. A one-point integration rule does not suffice, since it amounts to an averaging procedure which neglects all but the constant terms in the integrands of (2.18) and (2.23). Among the commonly known two-point quadrature methods, the Gaussian integration rule provides the highest accuracy when continuous functions are integrated. However, it introduces coupling between the degrees of freedom of adjacent nodal points along the fracture surfaces, (e.g. between the degrees of freedom of nodes 1 and 2 in Figure 2). This, in turn, can prevent the iterative solution algorithm from converging into dynamic states of equilibrium. For example, we tested the two-point Gaussian formulation in a series of problems which were supposed to simulate nonlinear displacement oscillations of a planar fault system in shear (i.e. frictional modes of deformation). The equilibrium iterations consistently failed to converge whenever one or more mass points passed the point of maximum amplitude and started to accelerate in reversed direction; see example 4 in Chapter 5. However, we have been able to simulate nonlinear frictional motions in a physically meaningful way by performing the state determination at the nodal points of the joint element. This was accomplished by choosing a two-point integration rule which samples at the two sections $\xi = \pm 1$. This integration rule is defined by the following example: consider the function $g(\xi)$, then

$$\int_{-1}^{1} g(\xi)\, d\xi \approx g(-1) + g(1) \quad . \tag{2.30}$$

The energies stored and dissipated in the joint element are determined by equations (2.27). The integrals in (2.27) are evaluated incrementally. For this purpose each integral in (2.27) is written in an incremental form which can be defined as follows:

$$\int_0^{\varepsilon} P(\varepsilon)\, d\varepsilon = \sum_{i=0,1,2,\ldots} \int_{\varepsilon_i}^{\varepsilon_{i+1}} P(\varepsilon)\, d\varepsilon \quad . \tag{2.33a}$$

The integrals extending over the individual increments are evaluated approximately using the trapezoidal rule:

$$\int_{\varepsilon_i}^{\varepsilon_{i+1}} P(\varepsilon)\, d\varepsilon \approx [P(\varepsilon_i) + P(\varepsilon_{i+1})](\varepsilon_{i+1} - \varepsilon_i)/2 \quad . \tag{2.33b}$$

Finally, it should be mentioned that the vector of nodal forces due to internal pressure, defined by (2.17) in conjunction with (2.29), is explicitly given by

$$\underset{\sim}{P} = \underset{\sim}{b}\, \underset{\sim}{p} \quad , \tag{2.34}$$

where

$$\underset{\sim}{p} = (p_1, p_2)^T \quad , \tag{2.35}$$

and $\underset{\sim}{b} = \underset{\sim}{N}\, \underset{\sim}{e}$. Matrix $\underset{\sim}{N}$ is defined by

$$\underset{\sim}{N} = \begin{bmatrix} -\underset{\sim}{n} & \underset{\sim}{0} \\ \underset{\sim}{0} & -\underset{\sim}{n} \\ \underset{\sim}{0} & \underset{\sim}{n} \\ \underset{\sim}{n} & \underset{\sim}{0} \end{bmatrix} \quad , \tag{2.36a}$$

where

$$\underset{\sim}{n} = (-\sin\Theta, \cos\Theta)^T \tag{2.36b}$$

is the unit vector in direction n (see Figure 2). Furthermore, matrix

The assemblage procedure establishing matrices $\underset{\sim}{M}$, $\underset{\sim}{K}$, $\underset{\sim}{B}$, etc. in terms of the corresponding element matrices is standard; see for example [12]. The initial value problem of (2.38) consists of finding the vector valued function $\underset{\sim}{u}(t)$ satisfying (2.38) at all times $t \in [0, t_{max}]$, $t_{max} > 0$ and

$$\left.\begin{aligned} \underset{\sim}{u}(0) &= \underset{\sim}{d} \\ \dot{\underset{\sim}{u}}(0) &= \underset{\sim}{v} \end{aligned}\right\} , \tag{2.40}$$

where $\underset{\sim}{d}$ and $\underset{\sim}{v}$ are given initial data. It is to be noted that the discrete model described by (2.38) dissipates energy through frictional deformations of the fracture surfaces only. Dissipation due to viscous properties of the material has been ignored.

Equation (2.38) constitutes one equation for the unknowns $\underset{\sim}{u}$ and $\underset{\sim}{H}$. To make the problem well posed a second equation is needed. It will be derived in the following chapter.

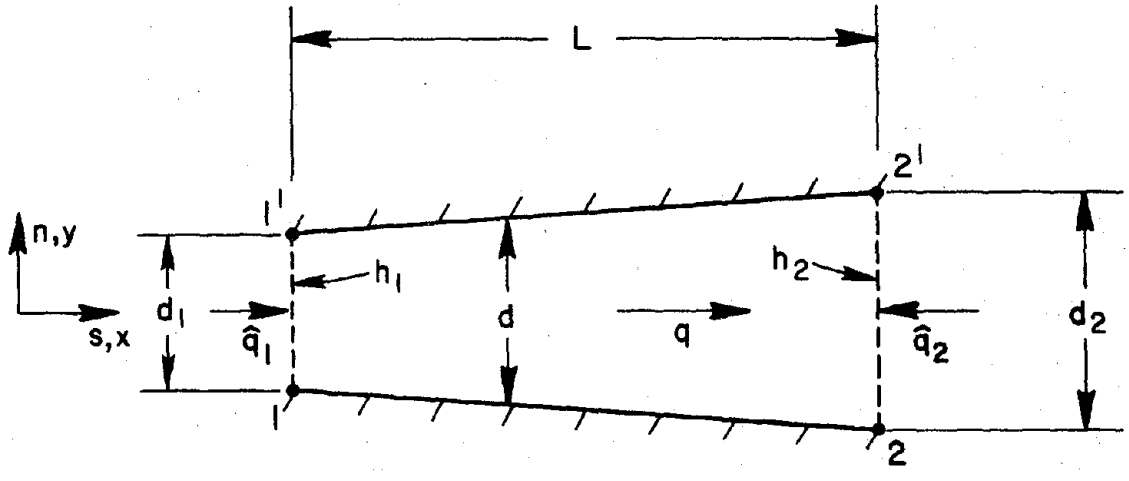

q = FLOW RATE (AVERAGED OVER THE CROSS-SECTION)
h = HEAD (AVERAGED OVER THE CROSS-SECTION)
d = WIDTH OF FLOW CHANNEL

Fig. 5. Geometry and coordinate system of a fluid flow element.

convective and inertia terms in the Navier-Stokes equation, for consistency, we also drop the kinetic energy term in the expression for p and simply use

$$p = \gamma h \quad . \tag{3.5}$$

Combining (3.3) and (3.4) yields the partial differential equation

$$\frac{\partial}{\partial x} \left(k \frac{\partial h}{\partial x}\right) = \frac{\partial S}{\partial t} \tag{3.6}$$

which determines the state of the fluid at any section x; see Figure 5. The boundary value problem consists of finding the function h(x,t) which satisfies (3.6) and one boundary condition at each end of the flow element depicted in Figure 5. Admissible boundary conditions are

$$\left.\begin{aligned} h = \hat{h}_1 \text{ or } q = \hat{q}_1 \quad &\text{at section 1} \\ h = \hat{h}_2 \text{ or } q = -\hat{q}_2 \quad &\text{at section 2} \end{aligned}\right\} \quad . \tag{3.7}$$

The sign convention used in (3.7) is defined in Figure 5, and prescribed quantities are characterized by a superposed hat.

In order to derive the finite element equations of the above boundary value problem, it has to be rewritten in weak form. Denoting the boundary points by "b", the points where q is specified by b_q and the prescribed boundary flow rates by $\hat{q}$, the weak (or Galerkin) form of (3.6) is given by

$$-\int_0^L \left[\frac{\partial}{\partial x} \left(k \frac{\partial h}{\partial x}\right) - \frac{\partial S}{\partial t}\right] \psi(x)\, dx + \oint_{b_q} (\hat{q}-q)\, \Psi(x)\, db = 0 \ , \tag{3.8}$$

which must hold for all admissible functions $\psi(x)$; see Strang and Fix [13]. The first step towards the discretization of (3.8) is to admit only a finite number of test functions $\psi_i(x)$. Here i = 1, 2 and the functions ψ_i are

$$\underset{\sim}{k}_F = \frac{\bar{k}}{L}\begin{bmatrix} 1 & -1 \\ -1 & 1 \end{bmatrix} \quad , \tag{3.14a}$$

$$\underset{\sim}{h} = (h_1, h_2)^T \quad , \tag{3.14b}$$

$$\underset{\sim}{q} = (q_1, q_2)^T \quad , \tag{3.14c}$$

$$\underset{\sim}{S} = (S_1, S_2)^T \quad . \tag{3.14d}$$

In (3.14a)

$$\bar{k} = \gamma A \bar{d}^3/(12\mu) \quad , \tag{3.14e}$$

where

$$\bar{d}^3 = (d_1^3 + d_1^2 d_2 + d_1 d_2^2 + d_2^3)/4 \quad . \tag{3.14f}$$

Note that the "hats" on the nodal quantities in (3.14b,c) are omitted for notational convenience.

A basic question with regard to the finite element fluid-flow equations is the following: Do equations (3.13) determine states of fluid flow which approximately (i.e. in a discrete fashion) satisfy the governing differential equation (3.6)? To answer this question we compare the sum and the difference of equations (3.13) with the associated differential equations (3.3) and (3.4), respectively. The sum yields

$$\frac{q_2 - q_1}{L} + \frac{\dot{S}_1 + \dot{S}_2}{2} = 0 \quad , \tag{3.15a}$$

and the difference can be written in the form

$$\bar{k} \quad \frac{h_2 - h_1}{L} + \frac{q_1 + q_2}{2} = L(\dot{S}_1 - \dot{S}_2)/12 \quad . \tag{3.15b}$$

Obviously, (3.15a) is a first order difference approximation to (3.3); (3.15b) is a first order difference formula for (3.4), provided that $L|\dot{S}_2 - \dot{S}_1|$ is sufficiently small compared to the left hand terms in (3.15b). Thus, the form (3.13) is consistent with (3.6) and the discrete solution converges to

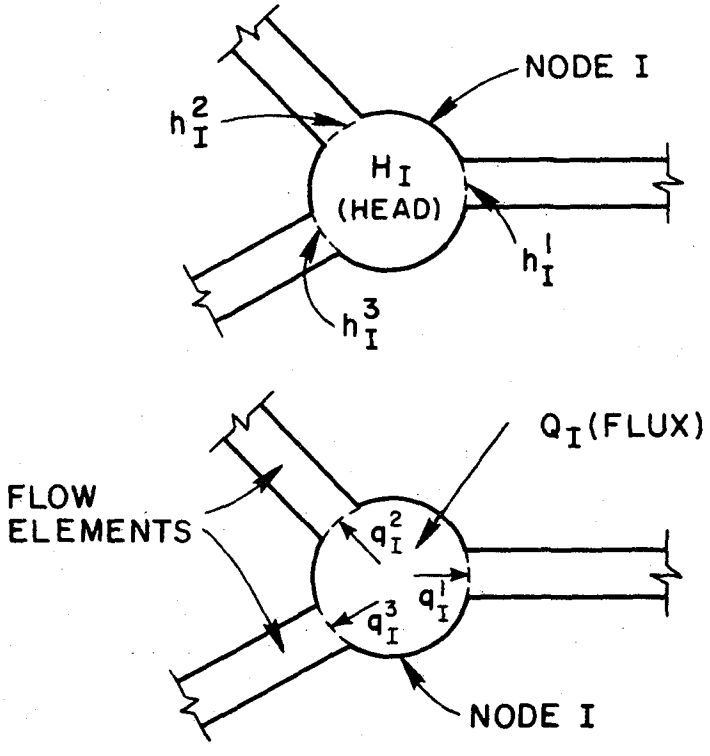

BALANCE OF MOMENTA AT NODE I:

$h_I^e = H_I \ (e = 1,2,3)$

BALANCE OF MASS AT NODE I:

$$\sum_{e=1}^{3} q_I^e = Q_I$$

FLOW BOUNDARY CONDITIONS REQUIRE EITHER H_I OR Q_I TO BE PRESCRIBED.

Fig. 6. Assembly conditions for fluid flow elements.

4. SOLUTION ALGORITHMS FOR THE NONLINEAR DYNAMIC STRESS-FLOW ANALYSIS

The behavior of the entire solid-fluid system of fractured rock is described by equations (2.38) and (3.20). The interactive effects between the solid and fluid domains in the model are represented by the term $\underset{\sim}{B}\,\underset{\sim}{H}$ in (2.38), and by the terms $\underset{\sim}{B}_F^T\,\dot{\underset{\sim}{u}}$ and $\underset{\sim}{K}_F\,\underset{\sim}{H}$ in (3.20). To determine the state of the system at all times $t \in (0, t_{max}]$ we have to find the response histories $\underset{\sim}{u}(t)$ and $\underset{\sim}{H}(t)$ which simultaneously satisfy equations (2.38) and (3.20). Due to the inherent complexity and nonlinearity of this sytem of coupled differential equations we cannot hope to find a closed form solution, but instead must resort to numerical techniques which generate approximate solutions in a step-by-step fashion.

4.1. TIME DISCRETIZATION

The Newmark family of step-by-step integration formulas [11] was found to be a versatile and efficient tool for integrating equations (2.38) and (3.20). Application of the Newmark methods amounts to replacing these differential equations by the following algebraic equations of recursive form:

$$\left.\begin{aligned} \underset{\sim}{d}_{n+1} &= \underset{\sim}{d}_n + \Delta t\, \underset{\sim}{v}_n + \Delta t^2[(1/2 - \beta)\, \underset{\sim}{a}_n + \beta\, \underset{\sim}{a}_{n+1}] \\ \underset{\sim}{v}_{n+1} &= \underset{\sim}{v}_n + \Delta t[(1 - \gamma)\, \underset{\sim}{a}_n + \gamma\, \underset{\sim}{a}_{n+1}] \end{aligned}\right\}, \qquad (4.1a)$$

$$\underset{\sim}{M}\,\underset{\sim}{a}_{n+1} + \underset{\sim}{K}(\underset{\sim}{d}_{n+1}) = \underset{\sim}{R}_{n+1} + \underset{\sim}{B}\,\underset{\sim}{H}_{n+1}, \qquad (4.1b)$$

$$\underset{\sim}{B}_F^T\,\underset{\sim}{v}_{n+1} + \underset{\sim}{K}_F(\underset{\sim}{d}_{n+1})\,\underset{\sim}{H}_{n+1} = \underset{\sim}{Q}_{n+1}, \qquad (4.1c)$$

$$\left.\begin{aligned} \underset{\sim}{d}_o &= \underset{\sim}{d} \\ \underset{\sim}{v}_o &= \underset{\sim}{v} \end{aligned}\right\}, \qquad (4.1d)$$

$$\left.\begin{aligned} \underset{\sim}{H}_o &= \underset{\sim}{K}_F^{-1}(\underset{\sim}{d}_o)\,[\underset{\sim}{Q}_o - \underset{\sim}{B}_F^T\,\underset{\sim}{v}_o] \\ \underset{\sim}{a}_o &= \underset{\sim}{M}^{-1}\,[\underset{\sim}{R}_o + \underset{\sim}{B}\,\underset{\sim}{H}_o - \underset{\sim}{K}(\underset{\sim}{d}_o)] \end{aligned}\right\}, \qquad (4.1e)$$

$$E_K^n = 1/2\ \underset{\sim}{v}_n^T\ \underset{\sim}{M}\ \underset{\sim}{v}_n \tag{4.4a}$$

and

$$U_s^n = 1/2\ \underset{\sim}{d}_n^T\ \underset{\sim}{K}_s\ \underset{\sim}{d}_n + \underset{\sim}{F}_s^T(\underset{\sim}{\sigma}_o)\ \underset{\sim}{d}_n \quad , \tag{4.4b}$$

respectively, where $\underset{\sim}{M}$ is the mass matrix of the solid material and $\underset{\sim}{K}_s$ is defined by (2.39). Both $\underset{\sim}{M}$ and $\underset{\sim}{K}_s$ are assembled from the mass and stiffness matrices of the isoparametric quadrilateral elements. The vector $\underset{\sim}{F}_s(\underset{\sim}{\sigma}_o)$ in (4.4b) represents the nodal forces due to the initial state of stress of the continuous rock. In (2.38) the effect of initial stresses is implicitly accounted for through $\underset{\sim}{R}$. In the computer program matrix operations (4.4) are most efficiently performed at the element level.

4.3 SOLUTION STRATEGY FOR THE ANALYSIS OF COUPLED SOLID-FLUID SYSTEMS

In order to generate the entire response history the system of nonlinear algebraic equations (4.2) has to be solved at the set of discrete points t_{n+1}, $n = 0,1,2, \ldots, N-1$. Thus, at any instant of time t_n, it is essentially the same problem that has to be solved as in the case of the steady-state analysis.

The fixed-point iteration technique which was used by Gale et al. [8] to simulate quasi-static processes was found to be suitable for the dynamic analysis also. This technique amounts to solving equations (4.2b) for $\underset{\sim}{H}_{n+1}$ with $\underset{\sim}{d}_{n+1}$ fixed, and then holding $\underset{\sim}{H}_{n+1}$ fixed during the iterative solution of (4.2a) for $\underset{\sim}{d}_{n+1}$. This cycle is repeated until convergence is reached. Convergence implies that the fluid pressure distribution is (numerically) compatible with the state of stress throughout the deformable rock.

We define the fixed point iteration technique by rewriting (4.2) in the form

For notational simplicity we rewrite (4.5a) in the form

$$\tilde{\underset{\sim}{F}}(\underset{\sim}{d}) - \underset{\sim}{R}^* = \underset{\sim}{0} \quad , \tag{4.6a}$$

in which $\underset{\sim}{d} = \underset{\sim n+1}{d^{j+1}}$,

$$\underset{\sim}{R}^* = \tilde{\underset{\sim n+1}{R}} + \underset{\sim}{B}\ \underset{\sim n+1}{H^j} \tag{4.6b}$$

and

$$\tilde{\underset{\sim}{F}}(\underset{\sim}{d}) = (\alpha_o\ \underset{\sim}{M} + \underset{\sim s}{K})\ \underset{\sim}{d} + \underset{\sim J}{K}(\underset{\sim}{d}) \quad , \tag{4.6c}$$

where $\underset{\sim s}{K}$ and $\underset{\sim J}{K}$ are defined by (2.39). To solve (4.6a) for $\underset{\sim}{d}$ we use the Newton-Raphson method; it is defined by the following recursive formulas:

$$\left.\begin{aligned} \underset{\sim}{DK}^i\ \underset{\sim}{\Delta d}^{i+1} &= \underset{\sim}{R}^* - \tilde{\underset{\sim}{F}}(\underset{\sim}{d}^i) \\ \underset{\sim}{d}^{i+1} &= \underset{\sim}{d}^i + \underset{\sim}{\Delta d}^{i+1} \end{aligned}\right\} \quad , \ i = 0,1,2,\ldots . \tag{4.7}$$

The starting values are given by $\underset{\sim}{d}^o = \underset{\sim n+1}{d^j}$, and the tangent stiffness matrix

$$\underset{\sim}{DK}^i = \alpha_o\ \underset{\sim}{M} + \underset{\sim s}{K} + \underset{\sim J}{DK}^i \quad , \tag{4.8a}$$

where

$$\underset{\sim J}{DK}^i = \left.\frac{\partial \underset{\sim J}{K}}{\partial \underset{\sim}{d}}\right|_{\underset{\sim}{d}=\underset{\sim}{d}^i} \quad . \tag{4.8b}$$

$\underset{\sim J}{DK}^i$ is assembled from the corresponding joint element stiffness matrices defined by (2.21). Equilibrium is achieved, and the iteration is terminated, if

$$||\underset{\sim}{R}^* - \tilde{\underset{\sim}{F}}(\underset{\sim}{d}^{i+1})||_2 < \varepsilon_s \quad , \tag{4.9a}$$

where $||\ldots||_2$ is the L_2 vector norm defined by $||\underset{\sim}{F}||_2 = (\sum_k F_k^2)^{1/2}$, $\underset{\sim}{F} = (F_1, F_2, \ldots)^T$, and ε_s is a given convergence tolerance. Instead of (4.9a) the following convergence criteria may be used:

$$||\underset{\sim}{\Delta d}^{i+1}||_2 < \varepsilon_s\ ||\underset{\sim}{d}^i||_2 \quad . \tag{4.9b}$$

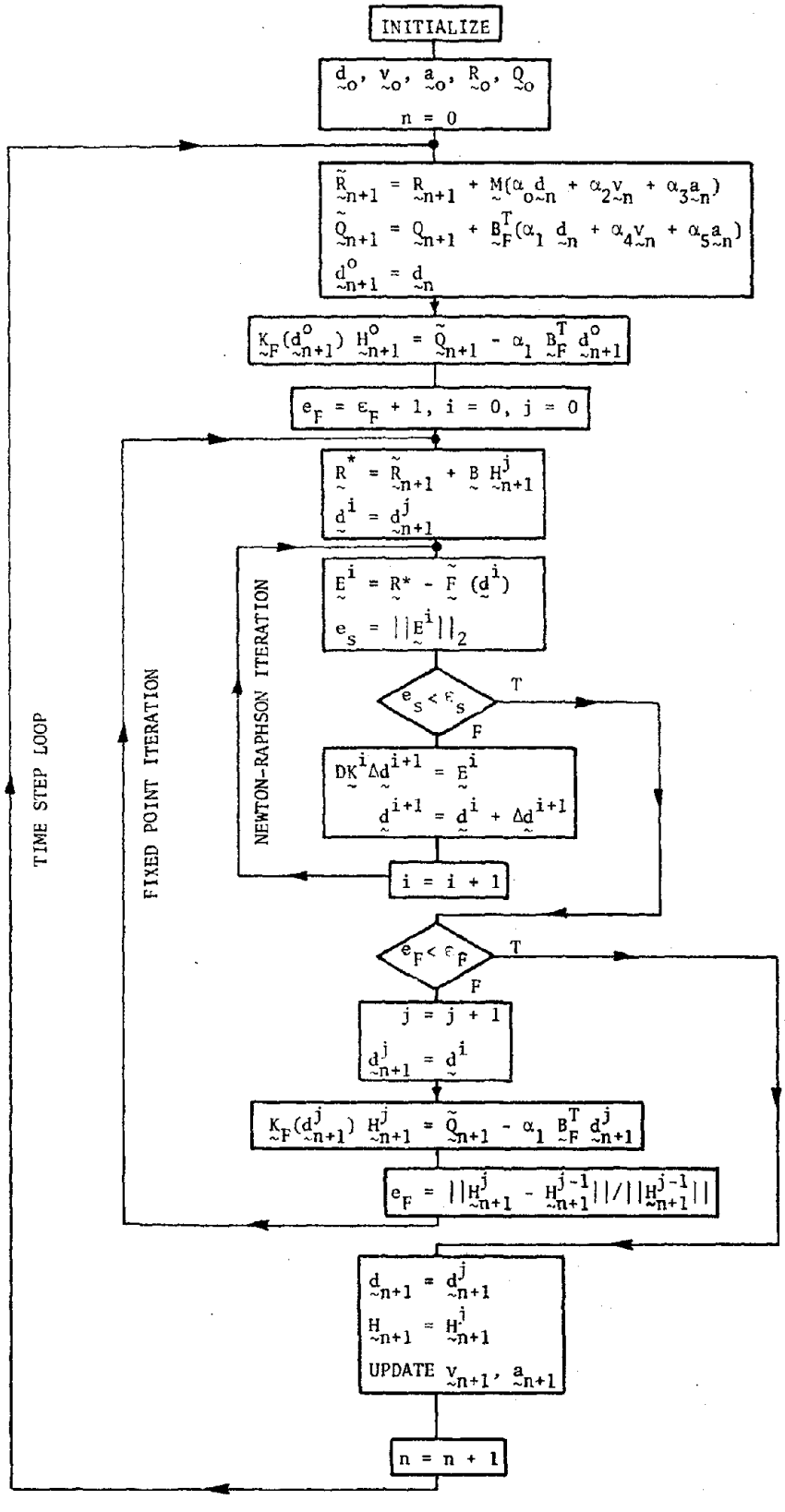

Fig. 7. Flow chart of the complete solution procedure for coupled stress-flow analysis.

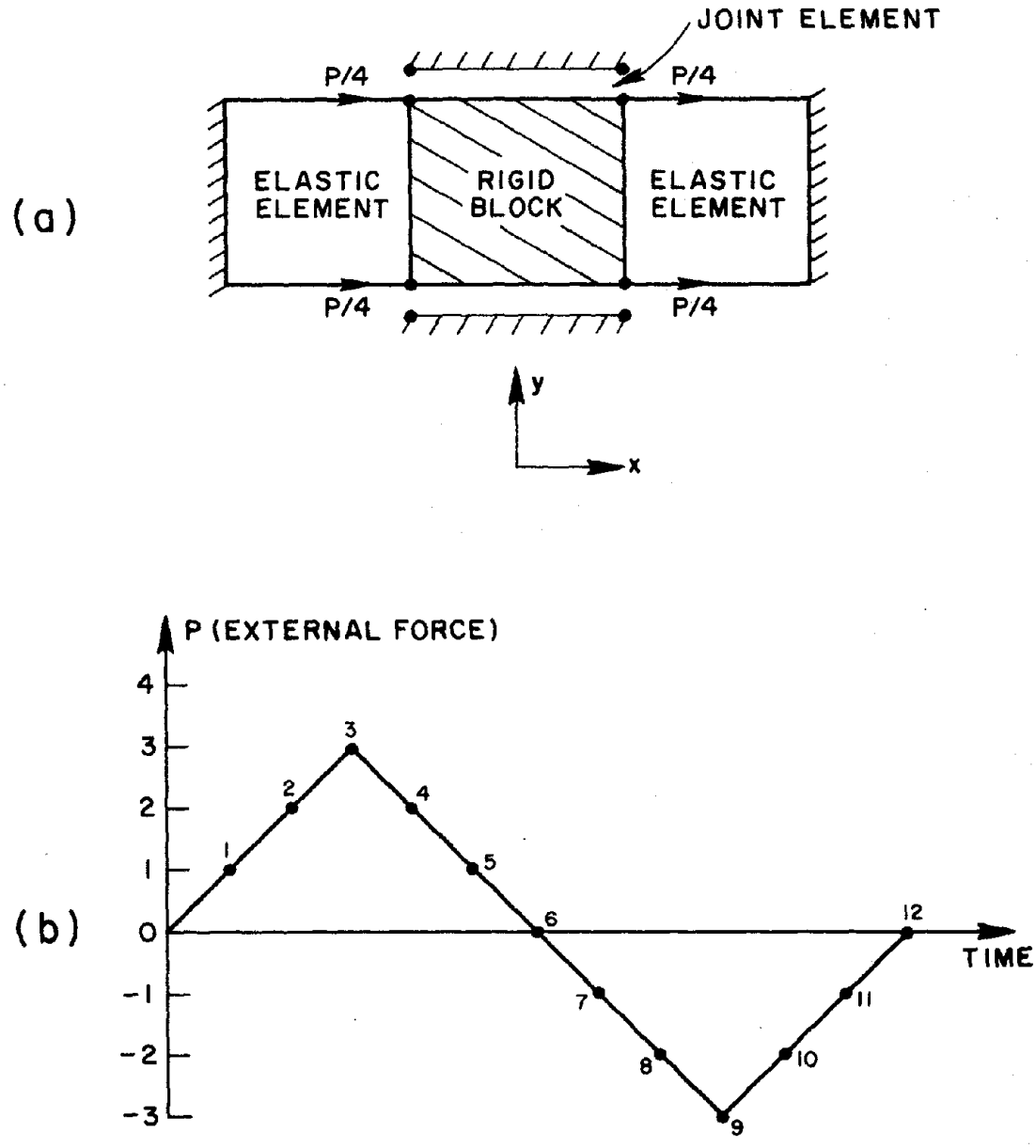

Fig. 8. Elastically supported rigid block sliding between joints in a quasi-static forced motion. (a) Problem set-up. (b) Forcing function.

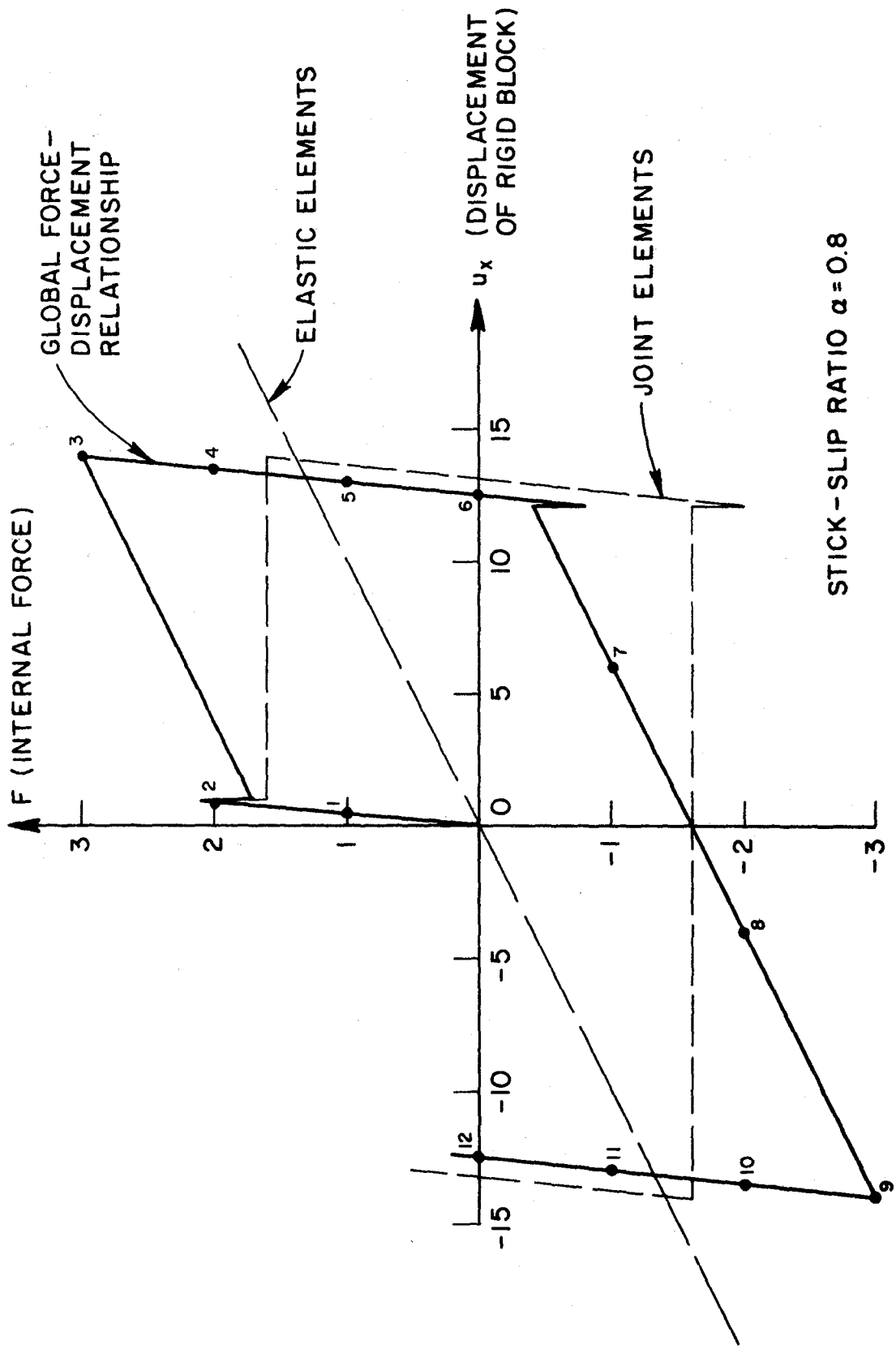

Fig. 9. Equilibrium configurations of rigid block in quasi-static forced motion.

5.2 SINGLE DEGREE-OF-FREEDOM OSCILLATORY SYSTEM

A single degree-of-freedom oscillatory system is used to test the release and locking mechanisms of the joint elements as well as the solution algorithms, under nonlinear dynamic conditions. The problem set-up is shown in Figure 11: A rigid block is sliding between two joints in a dynamic motion which consists of a forced and a free phase. The finite element mesh and the forcing function P(t) are defined in Figure 11.

The constitutive relations of the joint elements are defined in Figures 3 and 4 with the following data: $f_n = f_{no} = -1$, $f_{so} = 0$, $k_{no} = 1$, $k_{so} = 1/2$, $d_o = 1$, $\phi = 45°$, $C = 0$, $\alpha = 1$. The mass of the rigid block is assumed to be one and the time step size $\Delta t = 1/10$. Since $C = 0$ and $f_n = -1$, the peak shear strength f_{sy} equals one. As in the previous example, no fluid effects are considered. If the density of the fluid is set to zero, the computer program automatically skips the determination of the fluid flow and the fixed-point iteration is switched off.

The displacement of the rigid block as a function of time is shown in Figure 12. For the purpose of comparison, the displacement reponse history according to a linear joint constitutive law is included in the same figure. As indicated in Figure 11, the motion is forced during the first 3.4 seconds, and it is free thereafter. The amplitudes of the free oscillator can be read off Figure 12. They are $u_{max} = 4.3$ for linear elastic friction and $u_{max} - u_{steady\ state} = 2$ for the elastic-plastic friction mechanisms. The difference between the linear and the nonlinear oscillations is due to the energy dissipated during plastic sliding. The slip-phases are indicated in Figure 12, and the force-displacement history is plotted in Figure 13. Figures 12 and 13 indicate that the rigid mass slides into a new permanently displaced equilibrium position, $u_{steady\ state}$, about which it oscillates

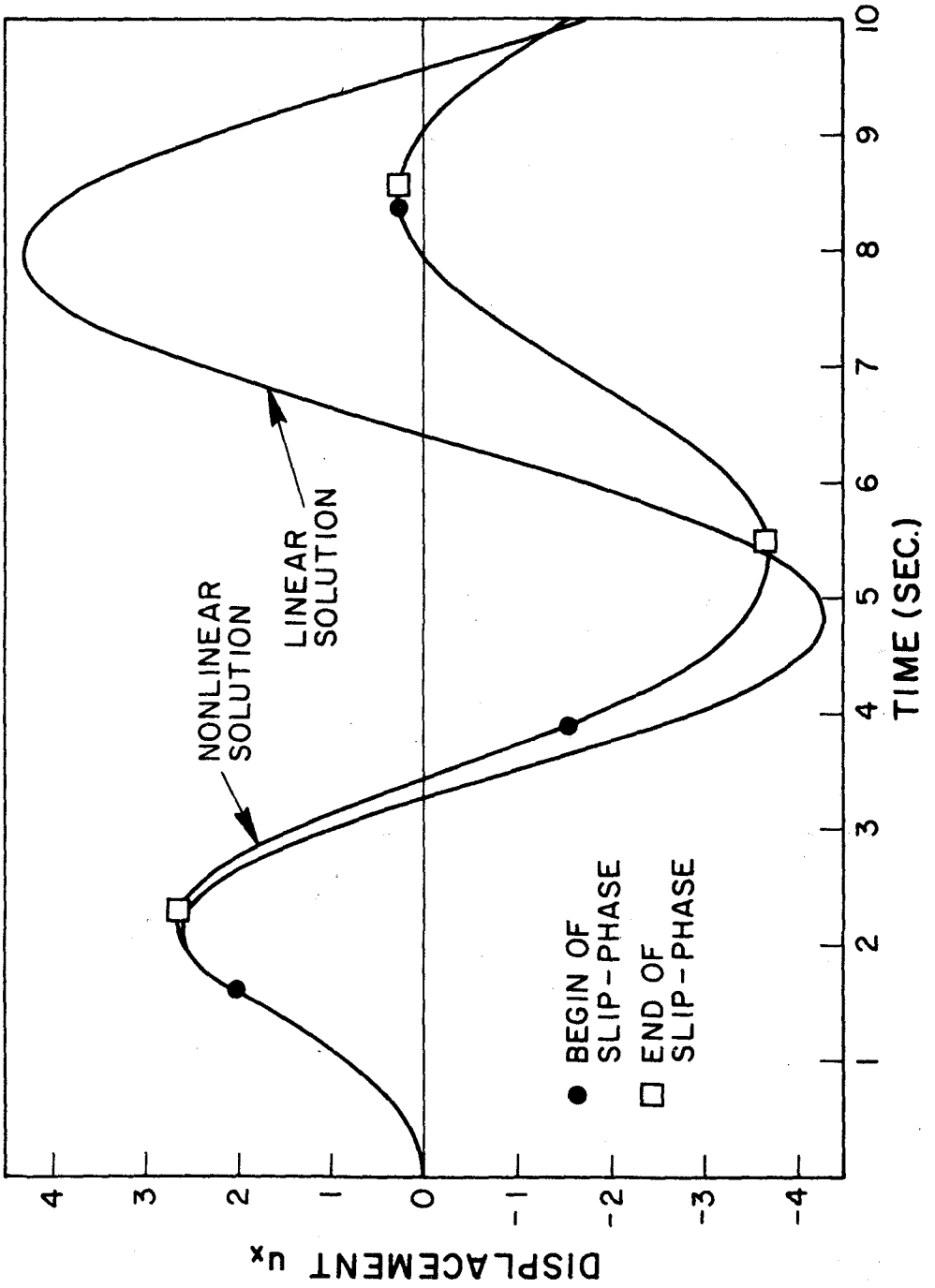

Fig. 12. Displacement response histories of rigid block oscillator.

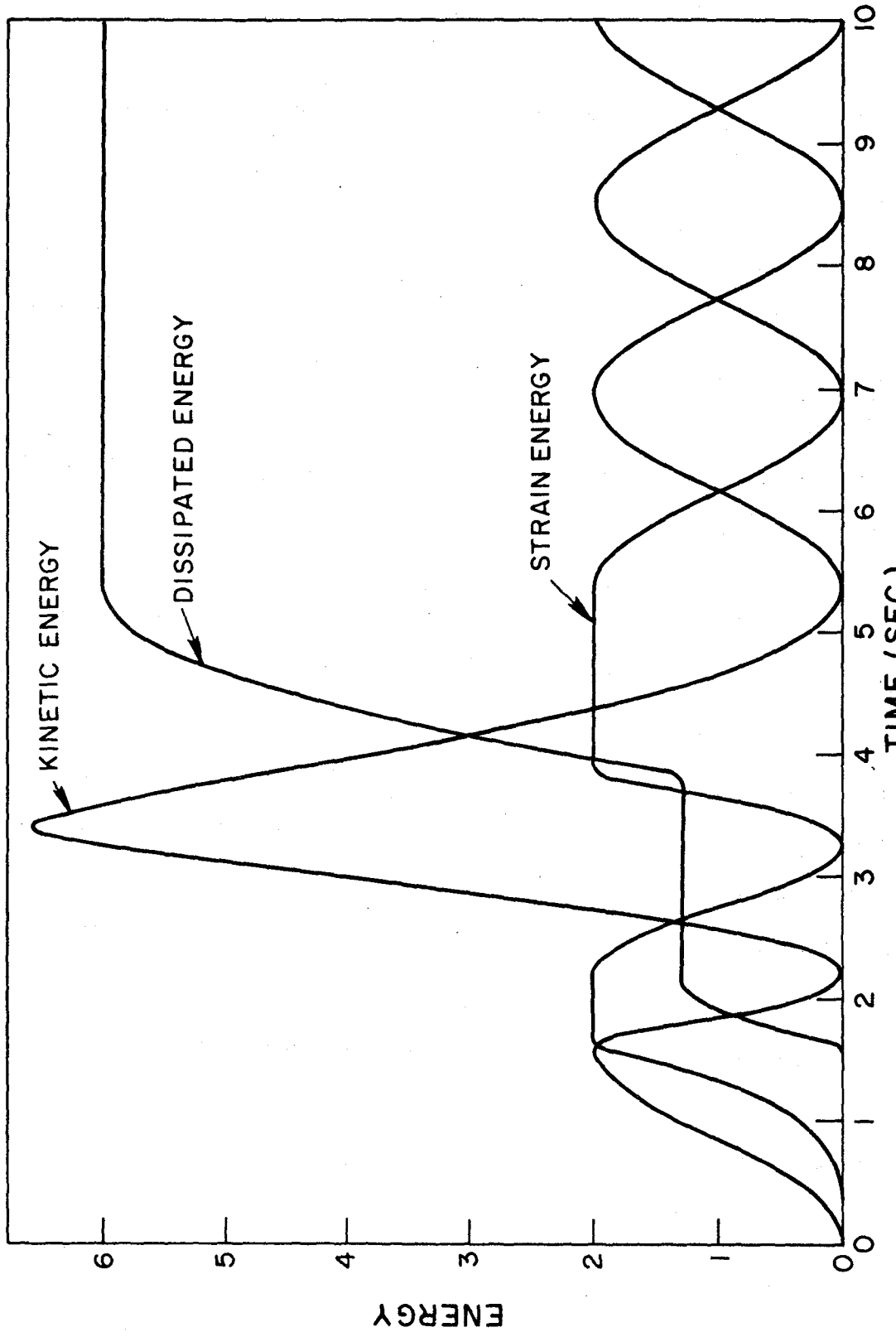

Fig. 14. Strain energy, kinetic energy and dissipated energy of the rigid block oscillator versus time.

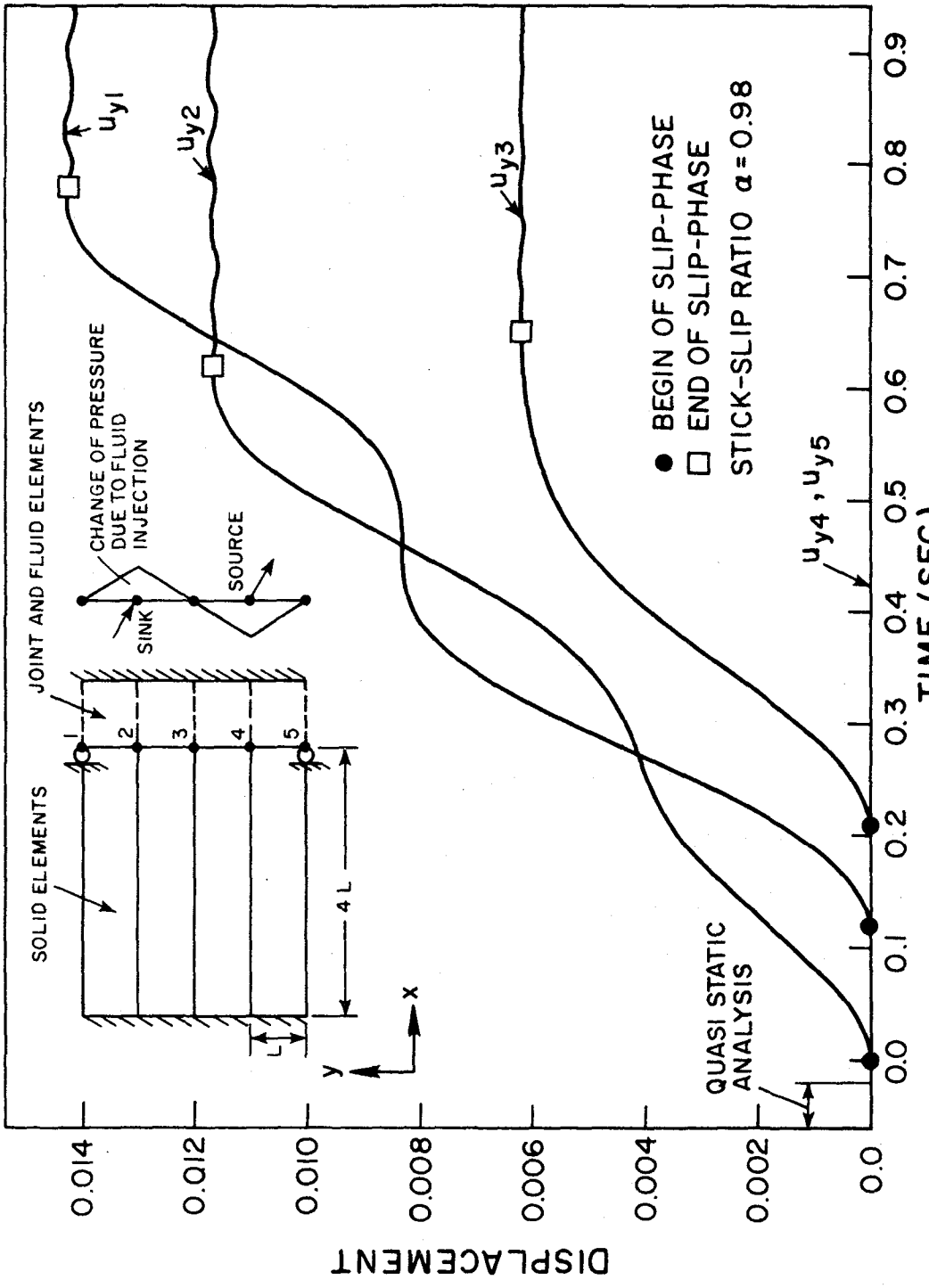

Fig. 15. General set-up of problem 3, and nodal displacements parallel to the fracture plane versus time.

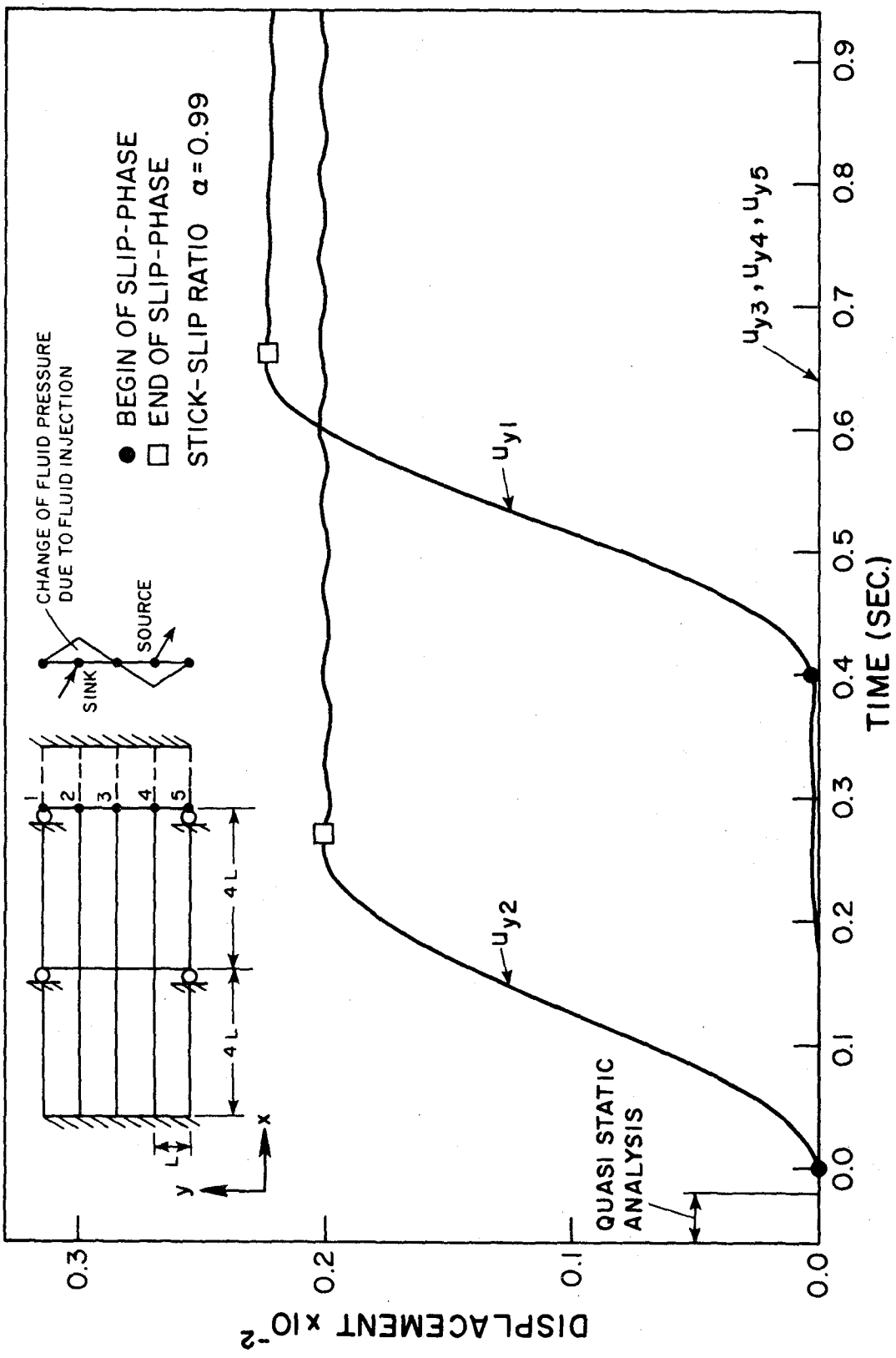

Fig. 16. General set-up of problem 4, and nodal displacements parallel to the fracture plane versus time.

stick-slip ratio $\alpha = 0.99$. The new mesh and the corresponding displacement histories $u_y(t)$ of nodes 1 and 2 are depicted in Figure 16. Figure 17 shows the displacement response histories of nodes 1, 2 and 3 in a larger scale. The final increase of pressure which was necessary to create failure at node 2 induced a vibration of nodes 2 and 4 in x-direction, as indicated in Figure 17. The motions of some points within the continuous rock are indicated in Figure 18, in which the response functions $u_y(t)$ of nodes 6, 7, 8 and 10 are plotted.

The original joint element, as introduced in [7], employes a one-point integration rule. It has been explained in Chapter 3, why this is inadequate in general: The one-point integration rule neglects the strain energy due to nonuniform deformation patterns. Hence, a joint element based on a two-point Gaussian integration rule was tested. However, this formula introduces coupling between the sections 1,4 and 2,3 of the joint element (see Figure 2), which, in turn, can cause the joint element to simulate friction and contact mechanisms in a physically incorrect way. For example, consider the displacement response histories of nodes 1 and 2 corresponding to the joint element with Gaussian integration, shown in Figure 19. The interaction between the degrees of freedom of adjacent nodes along the fault prevents the individual masses from being locked at the points of maximum displacement (i.e. zero velocity), and thus leads to physically meaningless results, as indicated in Figure 19.

5.5 EFFECT OF INJECTION AND WITHDRAWAL IN A CRUDE FRACTURE MODEL WITH STICK-SLIP RATIO OF 0.94.

In this example we consider a rigidly supported mass of rock, which is subdivided by a straight fracture into two equal parts. The finite element

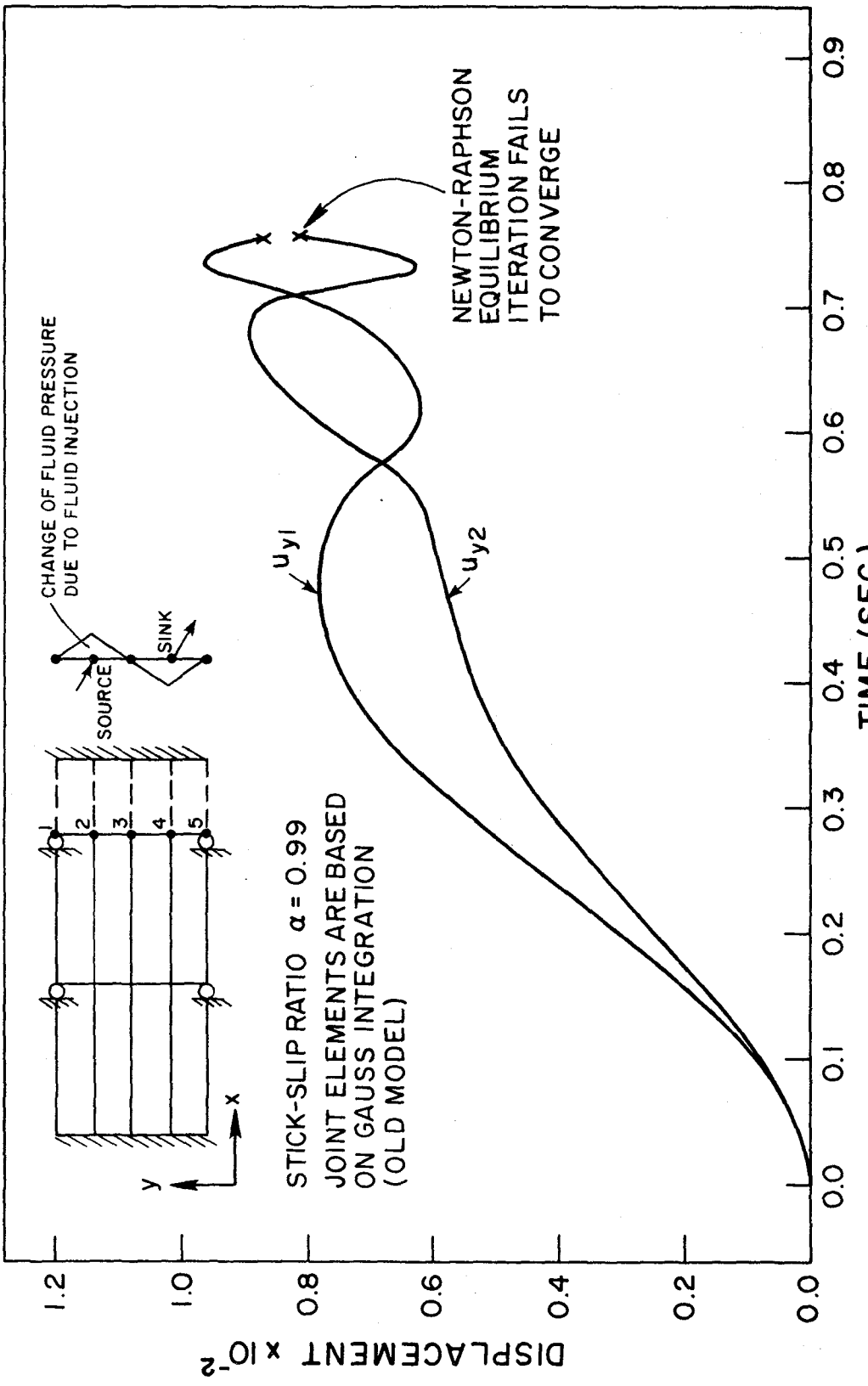

Fig. 19. Results generated by joint elements which are based on a two-point Gauss integration.

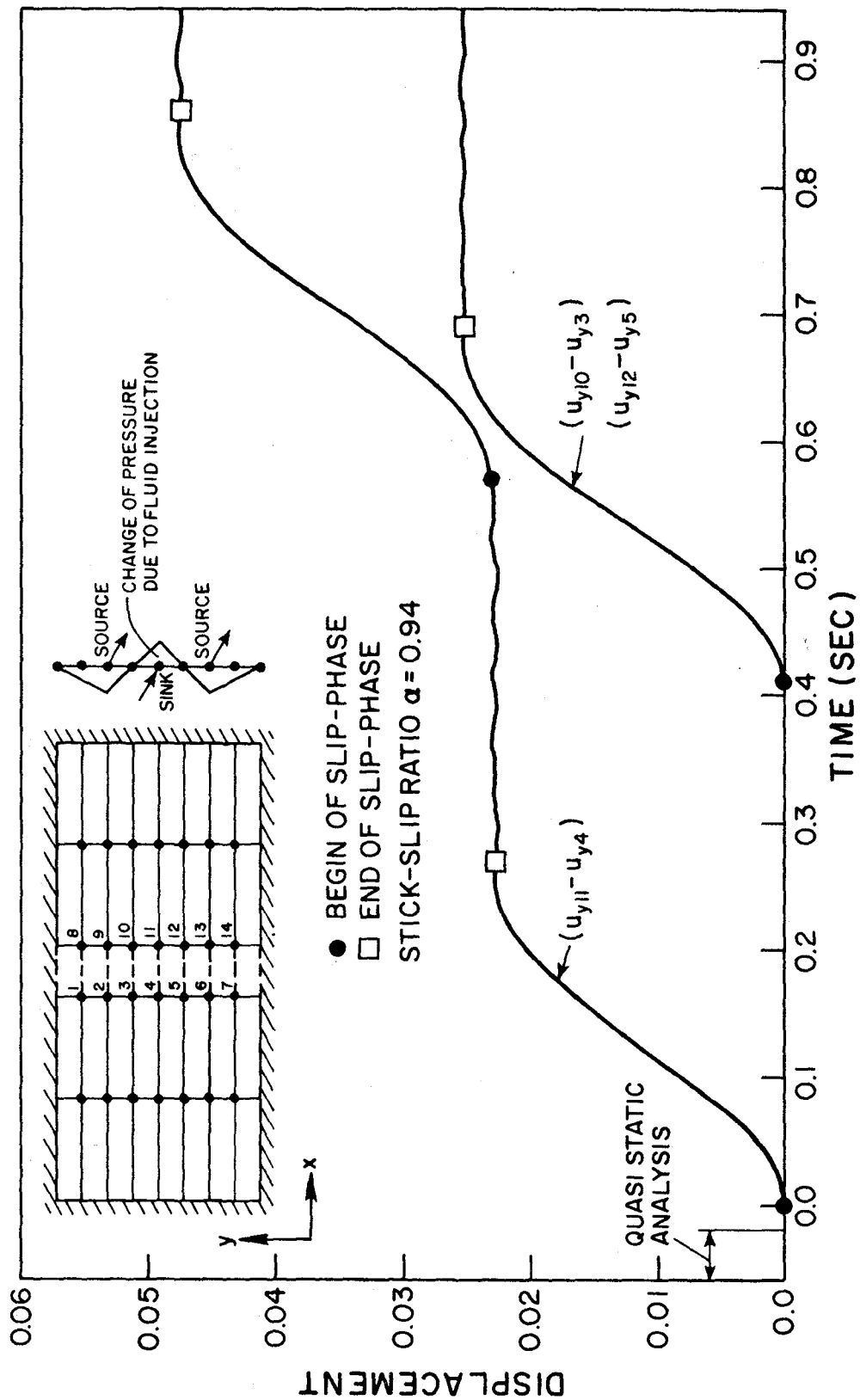

Fig. 20. Definition of problem 5, and displacement histories of some nodal points along the fault.

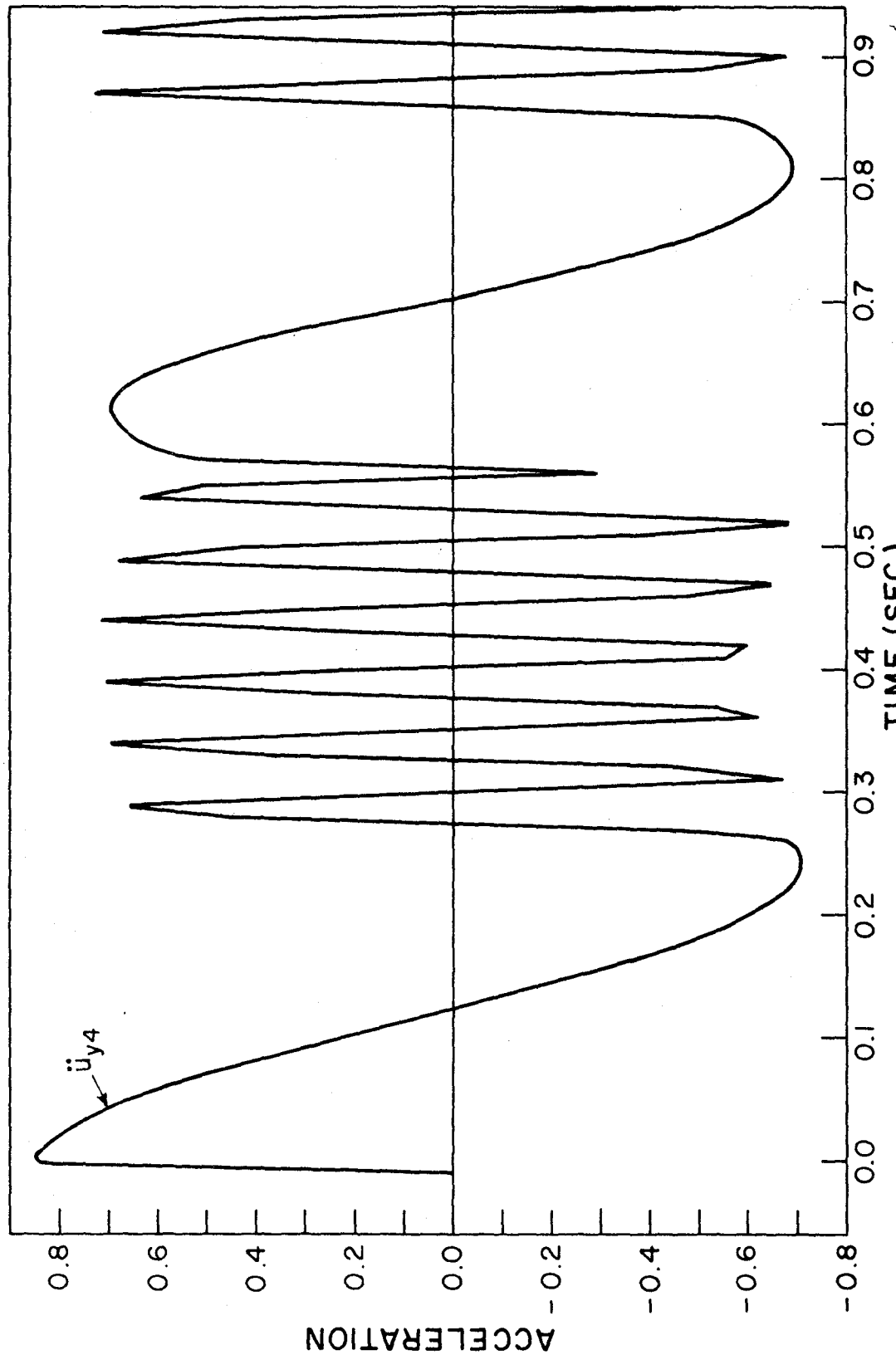

Fig. 22. Acceleration of node 4 in direction parallel to fault versus time.

The y-acceleration of nodal point 4 as function of time is plotted in Figure 22. The slip phases are clearly distinguished from the phases of linear elastic oscillations around the new positions of equilibrium indicated in Figure 20.

The energy dissipated during slip and the kinetic energy of the rock as functions of time are plotted in Figure 23. The change in strain energy of the system, denoted by ΔU^n can be computed from

$$E_D^n + E_K^n + \Delta U^n = E_{Ko} + \Delta U_o \ , \ n = 0,1,2,\ldots,N, \quad (5.2)$$

where E_{Ko} is the kinetic energy and ΔU_o is the change in strain energy at the instant of failure. In the present case $E_{Ko} + \Delta U_o = -0.5\ 10^4$.

REFERENCES

1. J. H. Dietrich, C. B. Raleigh and J. D. Bredehoeft, "Earthquake Triggering by Fluid Injection at Rangely, Colorado", Proceedings Symposium of International Society for Rock Mechanics, Percolation through Fissured Rock, Stuttgart, Germany, September 18-19, 1972.

2. J. H. Dietrich, "A Deterministic Near-Field Source Model",Proceedings Fifth World Conference on Earthquake Engineering, Rome, Italy, June 25-29, 1973.

3. J. Handin, and C. B. Raleigh, "Manmade Earthquakes and Earthquake Control", Proceedings Symposium of International Society for Rock Mechanics, Percolation through Fissured Rock, Stuttgart, Germany, September 18-19, 1972.

4. W. Rodatz and W. Wittke, "Wechselwirkung Zwischen Deformation und Durchströmung in Klüftigen, Anisotropen Gebirgen", Proceedings Symposium of International Society for Rock Mechanics, Percolation through Fissured Rock, Stuttgart, September 18-19, 1972.

5. N. R. Morgenstern and H. Guther, "Seepage into an Excavation in a Medium Possessing Stress-Dependent Permeability", Proceedings Symposium of International Society for Rock Mechanics, Percolation through Fissured Rock, Stuttgart, September 18-19, 1972.

6. J. Noorishad, P. A. Witherspoon and T. L. Brekke, "A Method for Coupled Stress and Flow Analysis of Fractured Rock Masses", Geotechnical Engineering Report No. 71-6, University of California, Berkeley, 1971.

7. R. E. Goodman, R. L. Taylor and T. L. Brekke, "A Model for the Mechanics of Jointed Rock", J. Soil Mech. Found. Div., Proc. ASCE, SM3, pp. 637-659, 1968.

8. J. E. Gale, R. L. Taylor, P. A. Witherspoon and M. S. Ayatollahi, "Flow in Rocks with Deformable Fractures", Proc. Int. Symposium on Finite Element Methods in Flow Problems, Swansea, United Kingdom, 1974, UAH Press, The University of Alabama in Huntsville, 1974.

9. R. E. Goodman and J. Dubois, "Duplication of Dilatancy in Analysis of Jointed Rocks", J. Soil Mech. Found. Div., Proc. ASCE, SM4, pp. 399-422, 1972.

10. J. Ghaboussi, E. L. Wilson and J. Isenberg, "Finite Element for Rock Joints and Interfaces", J. Soil Mech. Found. Div., Proc. ASCE, SM10, pp. 833-848, 1973.

11. G. L. Goudreau and R. L. Taylor, "Evaluation of Numerical Integration Methods in Elastodynamics", Computer Meth. Appl. Mech. and Eng. 2, pp. 69-97, 1973.